Luminosity-Independent Measurement of the Proton-Proton Total Cross Section at $\sqrt{s} = 8$ TeV

G. Antchev *et al.**
(TOTEM Collaboration)

The TOTEM collaboration has measured the proton-proton total cross section at $\sqrt{s} = 8$ TeV using a luminosity-independent method. In LHC fills with dedicated beam optics, the Roman pots have been inserted very close to the beam allowing the detection of ~90% of the nuclear elastic scattering events. Simultaneously the inelastic scattering rate has been measured by the T1 and T2 telescopes. By applying the optical theorem, the total proton-proton cross section of (101.7 ± 2.9) mb has been determined, well in agreement with the extrapolation from lower energies. This method also allows one to derive the luminosity-independent elastic and inelastic cross sections: $\sigma_{el} = (27.1 \pm 1.4)$ mb; $\sigma_{inel} = (74.7 \pm 1.7)$ mb.

PACS numbers: 13.85.Lg

Introduction.—The measurements at the ISR [1–3] (for proton-proton), at the $S\bar{p}pS$ [4] collider, and at the TEVATRON [5,6] (for proton-antiproton) have provided a clear evidence of the rise of the total cross section with energy. The CERN Large Hadron Collider (LHC) with its energy reach up to 14 TeV and an unprecedented dedicated forward-detector system operated by the TOTEM collaboration provides the unique opportunity to precisely determine σ_{tot} at various energies and thus the functional form of the rise with energy.

This Letter presents the first luminosity-independent measurement of the total proton-proton cross section at the LHC at a center of mass energy $\sqrt{s} = 8$ TeV. The TOTEM collaboration has already measured the total proton-proton cross section at $\sqrt{s} = 7$ TeV and has demonstrated the reliability of the luminosity-independent method by comparing several approaches to determine the total cross sections [7,8]. The method requires the simultaneous measurements of the inelastic and elastic rates, as well as the extrapolation of the latter in the invisible region down to $|t| = 0$ [see Eq. (3)]. This is achieved with the TOTEM experimental setup which consists of two inelastic telescopes T1 and T2 to detect charged particles produced in inelastic pp collisions, and Roman pot stations to detect elastically scattered protons at very small angles.

The telescopes consists of two arms placed symmetrically on both sides of interaction point 5 (IP5): the T1 telescope is based on cathode strip chambers (CSCs) placed at ± 9 m and covers the pseudorapidity range $3.1 \leq |\eta| \leq 4.7$; the T2 telescope is based on gas electron

multiplier (GEM) chambers placed at ± 13.5 m and covers the pseudorapidity range $5.3 \leq |\eta| \leq 6.5$. The pseudorapidity coverage of the two telescopes allows the detection of 95% of the inelastic events, including events with diffractive mass down to 3.6 GeV. As the fraction of events with all final state particles beyond the instrumented region has to be estimated using phenomenological models, the excellent acceptance in TOTEM allows a minimal dependence on such models and thus small uncertainty on the inelastic rate measurement.

Also, Roman pot (RP) stations are located symmetrically on either side of the IP at distances of 215–220 m from IP5. Each station is composed of two units separated by a distance of about 5 m. A unit consists of 3 RPs, two approaching the outgoing beam vertically and one horizontally. Each RP is equipped with a stack of 10 silicon strip detectors designed with the specific objective of reducing the insensitive area at the edge facing the beam to only a few tens of micrometers. The long lever arm between the near and the far RP units has two important advantages: the local track angles in the x and y projections perpendicular to the beam direction can be reconstructed with a precision of ~10 μrad and a high trigger efficiency ($> 99\%$) can be achieved as the proton trigger selection uses all RPs independently. A complete description of the TOTEM detector layout is given in [9].

Data taking.—The analysis presented in this Letter is performed on two data samples recorded in July, 2012 during two special LHC fills with $\beta^* = 90$ m optics. This special optics is described in detail in [7,10]. It has been successfully implemented and commissioned at the new LHC energy of 8 TeV keeping unchanged its main properties at the Roman pot stations located at 220 m: a large effective length, L_y, parallel-to-point focusing in the vertical plane and a very low effective length, L_x in the horizontal plane. These settings optimize the detection of elastic events and their separation from diffractive events. Both data samples consist of events triggered on: (i) one

---

*Full author list given at the end of the article.

TABLE I. Description of the available data samples. The RP position is given as the RP approach to the beam in multiples of the transverse beam size ($\sigma_{beam} \sim 0.7$ mm). The third column shows the lowest $|t|$ values reached in the elastic sample after all cuts. The last two columns show the number of elastic and inelastic events collected.

Data set	RP position	$|t|_{min}$ (GeV^2)	Elastic events	Inelastic events
1	$6.0\sigma_{beam}$	0.01	416×10^3	2.30×10^6
2	$9.5\sigma_{beam}$	0.02	238×10^3	1.72×10^6

colliding bunch-pair with a population of 7×10^{10} protons/bunch giving an instantaneous luminosity of $\approx 10 \, \text{mb}^{-1}\text{s}^{-1}$ and an average number of inelastic interactions of 0.05–0.06 per bunch crossing; (ii) one noncolliding bunch in each beam with the same population as the colliding ones.

The collected events have been triggered by the T2 telescope in either arm (inelastic trigger), by the RP detectors in a double-arm coincidence (elastic trigger), and by random bunch crossings (zero-bias sample used for calibration). A summary of the data samples is given in Table I.

Analysis: Elastic scattering.—The analysis follows the same procedure as the one performed for the measurement of the elastic cross section at 7 TeV [10]. The measurement of the elastic rate is based on the selection of events with the following topology in the RP detector system: a reconstructed track in the near and far vertical detectors on each side of the IP such that the elastic double-arm signature is satisfied in one of the two diagonals (left top and right bottom or left bottom and right top). Moreover, "elastic tagging" cuts (enforcing the elastic scattering kinematics constraints) are applied to suppress any background to a negligible level ($< 0.1\%$). Using the optical functions, the kinematics of the process is resolved and the differential rate is established as a function of the squared four-momentum transfer, t. After applying corrections that take into account acceptance limitations, resolution effects and

detector and reconstruction inefficiencies, it is possible to extrapolate the differential rate to $t = 0$.

The two data sets (each with two diagonals) are analyzed separately and the final results are combined only at the end, giving a better control over the systematics.

The key analysis steps are mentioned in more detail below, and they are quantified in Table II together with their systematic uncertainties.

Alignment: After applying all the alignment methods the residual misalignment is about 10 μm in the horizontal coordinate and about 50 μm in the vertical. When propagated to the reconstructed scattering angles, this leads to uncertainties of about 3 μrad (horizontal angle) and 0.1 μrad (vertical angle).

Elastic tagging: The event selection requires the colinearity of the two outgoing protons, the suppression of the diffractive events and the comparison of the horizontal vertex position reconstructed from the left and right arms. This last cut is very effective in suppressing beam-halo background. The cut thresholds were optimized for purity (background contamination in the selected sample less than 0.1%) and for efficiency (uncertainty of true elastic event selection 0.5%).

Kinematics reconstruction: The horizontal and vertical scattering angles (θ_x^*, θ_y^*) are reconstructed in each arm as [11]:

$$\theta_y^* = \frac{y}{L_y}, \qquad \theta_x^* = \frac{1}{dL_x/ds}\left(\theta_x - \frac{dv_x}{ds}x^*\right), \qquad (1)$$

where s denotes the distance from the interaction point, y the vertical displacement at the detector, θ_x the horizontal angle of the proton trajectory at the detector, and x^* the horizontal vertex coordinate. The settings of the LHC magnet lattice determine the betatron amplitude ($\beta^* = 90$ m at the IP) and the optical functions $L(s)_{x,y}$ and $v(s)_{x,y}$ (at $s = 220$ m: $L_y \approx 260$ m, $dv_x/ds \approx -0.05 \, \text{m}^{-1}$ and $dL_x/ds \approx -0.5$). The term with x^* is eliminated once the correlation between the left and right outgoing protons

TABLE II. Overview of the analysis steps, associated corrections, and systematic uncertainties to the differential and total elastic rate.

Source	Effect on	$|t| = 0.01$ GeV^2	0.1 GeV^2	0.2 GeV^2
Alignment	t	$\pm 0.21\%$	$\pm 0.3\%$	$\pm 0.57\%$
Kinematics reconstruction: Optics, beam energy	t	$\pm 1.09\%$	$\pm 0.72\%$	$\pm 4.3\%$
Selection	norm.		$\pm 0.5\%$	
Acceptance (correction factor)	dN/dt	3.3 ± 0.024	1.2 ± 0.002	1.8 ± 0.004
Resolution unfolding	t	$(0.5 \pm 0.1)\%$	$(-0.2 \pm 0.003)\%$	$(-2.6 \pm 0.1)\%$
Efficiency	norm.	Uncorrelated inefficiency: $(10 \pm 0.6)\%$ Correlated inefficiency: $(3 \pm 1)\%$ Pileup: $(4.7 \pm 0.4)\%$		
Extrapolation/Fit	$dN_{el}/dt|_{t=0}$ B		$\pm 2.5\%$ (19.9 ± 0.3) GeV^{-2}	

is enforced. The statistical uncertainty of the scattering angles is 2.2 μrad in the y projection (mainly due to the beam divergence) and 6.4 μrad in the x projection (due to the beam divergence and sensor pitch). The systematic uncertainties of the optical functions are about 1.5% for dL_x/ds and 0.4% for L_y, independently for each beam. These resolutions are then improved by a factor $\sqrt{2}$ when the left and right arm measurements are averaged.

Acceptance correction: Due to the detector shape and the LHC aperture, a geometrical acceptance correction is applied. The smearing around the acceptance limits (due to the beam divergence) is also taken into account and gives the only uncertainty of the acceptance correction. However, since the beam-divergence can be experimentally determined, the propagated uncertainty is small. The final t range is constrained to a region where the acceptance correction factor is below 5 in order to limit the systematic error on the final cross section.

Unfolding of resolution effects: The impact of resolution effects is assessed and eliminated exploiting a data-tuned Monte Carlo simulation. The angular spread is determined (by comparing the angles reconstructed from the left and right arm) with a small uncertainty (0.2 μrad), therefore the unfolding correction factors can be calculated with a precision better than 0.1%.

Efficiency: The detector reconstruction efficiency per RP is evaluated directly from the data. The source of inefficiencies, once acceptance effects have been excluded, is mainly the lack of capability of the strip detectors to resolve multiple tracks. These can be caused by interactions of the protons with the sensors or the surrounding material or by the overlap with beam halo protons. In Table II the corrections are listed in different categories: "uncorrelated," when one pot out of four has no reconstructed track; "correlated," when a shower originating in the near pot causes the loss of the track in one station; and "pileup" when one or more beam halo protons coincide with an elastic event.

Extrapolation to $t = 0$: The measured differential rate can well be described ($\chi^2/\text{ndf} \approx 1.1$) over the $|t|$ range from $|t|_{\min}$ to 0.2 GeV^2 by an exponential function with slope $B = (19.9 \pm 0.3)$ GeV^{-2}:

$$\frac{dN_{\text{el}}}{dt} = \frac{dN_{\text{el}}}{dt}\bigg|_{t=0} e^{-B|t|}. \qquad (2)$$

The stability of the fit has been verified by varying the lower $|t|$ bound. The observed systematic effect on the slope and the intercept is negligible compared to the other systematic uncertainties listed in Table II. Assuming that parametrization (2) holds also for $|t| < |t|_{\min}$, the value $dN_{\text{el}}/dt|_{t=0}$ can be used to determine the total cross section using Eq. (3). The measurements performed at very high β^* optics will allow the exploration of the $|t|$ region below the present $|t|_{\min}$ to seek the Coulomb-nuclear interference or any other new effect.

Elastic rate: The total nuclear elastic rate N_{el} is obtained by the integration of the data up to $|t| = 0.4$ GeV^2. The contribution due to events with larger $|t|$ is negligible ($< 0.1\%$) compared to the other uncertainties.

Systematic uncertainties: Monte Carlo techniques are used to study and evaluate the combined effect of the above mentioned systematic uncertainties. The leading effect is the uncertainty of the optics in the horizontal projection. However, the induced error changes sign at $|t| \approx 0.07$ GeV^2 which leads to partial error cancellation in the integrated elastic rate N_{el}.

Analysis: Inelastic scattering.—The analysis procedure is equivalent to the one performed for the measurement of the inelastic cross section at 7 TeV [12]. The observed inelastic rate is the number of events triggered by the T2 detector. The events are classified according to their topology: events with tracks in T2 in both hemispheres (2h), dominated by nondiffractive minimum bias and double diffractive processes, and events with tracks in one hemisphere only (1h) dominated by a single diffraction process. Several corrections have to be applied in order to derive the total inelastic rate. First, to obtain the visible rate, the observed rate is corrected for the trigger and detector efficiency, the background due to beam gas is subtracted, and the effect of the pileup is taken into account. Second, the rate corresponding to the events with at least one final state particle in $|\eta| < 6.5$ ($N_{|\eta|<6.5}$) is derived by taking into account the topologies which can cause an undetected event in T2. These are: events recorded only by T1, events with a rapidity gap covering T2, and central diffraction events with final states only in the central or very forward region. Third, to estimate the total inelastic rate N_{inel}, the contribution of low mass diffractive processes producing only final state particles at pseudorapidities above 6.5 is evaluated using Monte Carlo simulation. The main corrections which lead to the measurement of the total inelastic rate are described below and quantified in Table III together with their systematic uncertainties.

Beam gas background: This correction is estimated from events triggered on the noncolliding bunches. It is

TABLE III. Overview of the corrections and systematic uncertainties of the inelastic rate measurement. The second column shows the size of the correction, the third column the systematic uncertainty related to the source.

Source	Correction	Uncertainty	Effect on
Beam gas	0.45%	0.45%	all rates
Trigger efficiency	1.2%	0.6%	all rates
Pileup	2.8%	0.6%	all rates
T2 reconstruction	0.35%	0.2%	$N_{\text{inel}}, N_{|\eta|<6.5}$
"T1 only"	1.2%	0.4%	$N_{\text{inel}}, N_{|\eta|<6.5}$
Internal gap covering T2	0.4%	0.2%	$N_{\text{inel}}, N_{|\eta|<6.5}$
Central diffraction	0%	0.35%	$N_{\text{inel}}, N_{|\eta|<6.5}$
Low mass diffraction	4.8%	2.4%	N_{inel}

TABLE IV. Summary of the measured cross sections with detailed uncertainty composition. The ρ uncertainty follows from the COMPETE preferred-model ρ extrapolation error of ± 0.007. The right-most column gives the full systematic uncertainty, combined in quadrature and considering the correlations between the contributions.

Quantity	Value	Systematic uncertainty				
		el. t-dep	el. norm	inel	ρ	$\Rightarrow$ full
σ_{tot} (mb)	101.7	± 1.8	± 1.4	± 1.9	± 0.2	$\Rightarrow \pm 2.9$
σ_{inel} (mb)	74.7	± 1.2	± 0.6	± 0.9	± 0.1	$\Rightarrow \pm 1.7$
σ_{el} (mb)	27.1	± 0.5	± 0.7	± 1.0	± 0.1	$\Rightarrow \pm 1.4$
$\sigma_{\text{el}}/\sigma_{\text{inel}}$ (%)	36.2	± 0.2	± 0.7	± 0.9		$\Rightarrow \pm 1.1$
$\sigma_{\text{el}}/\sigma_{\text{tot}}$ (%)	26.6	± 0.1	± 0.4	± 0.5		$\Rightarrow \pm 0.6$

extracted and applied as a function of the T2 track multiplicity and affects only the 1h category. The systematic uncertainty is estimated to be 0.45% which corresponds to the maximal variation of the background that gives a compatible fraction of 1h events (trigger and pileup corrected) in the two samples.

Trigger efficiency: This correction is estimated from the zero-bias triggered events. It is extracted and applied as a function of the T2 track multiplicity, being significant for events with only one track and rapidly decreasing to zero for five or more tracks. The systematic uncertainty is evaluated comparing the trigger performances with and without the requirement of having a track pointing to the vertex and comparing the overall rate correction in the two samples.

Pileup: This correction factor is determined from the zero-bias triggered events: the probability to have a bunch crossing with tracks in T2 is 0.05–0.06 from which the probability of having $n \geq 2$ inelastic collisions with tracks in T2 in the same bunch crossing is derived. The systematic uncertainty is assessed from the variation, within the same data set, of the probability to have a bunch crossing with tracks in T2 and from the uncertainty due to the T2 event reconstruction efficiency.

Reconstruction efficiency: This correction is estimated using Monte Carlo generators (PYTHIA8 [13], QGSJET-II-03 [14]) tuned with data to reproduce the measured fraction of 1h events which is equal to 0.216 ± 0.007. The systematic uncertainty is assumed to be half of the correction: as it mainly depends on the fraction of events with only neutral particles in T2, it accounts for variations between the different Monte Carlo generators.

T1 only: This correction takes into account the amount of events with no final state particles in T2 but one or more tracks in T1. The uncertainty is the precision with which this correction can be calculated from the zero-bias sample plus the uncertainty of the T1 reconstruction efficiency.

Internal gap covering T2: This correction takes into account the events which could have a rapidity gap fully covering the T2 η range and no tracks in T1. It is estimated from data, measuring the probability of having a gap in T1

and transferring it to the T2 region. The uncertainty takes into account the different conditions (average charged multiplicity, p_T threshold, gap size, and surrounding material) between the two detectors.

Central diffraction: This correction takes into account events with all final state particles outside the T1 and T2 pseudorapidity acceptance and it is determined from simulations based on the PHOJET and MBR event generators [15,16]. Since the cross section is unknown and the uncertainties are large, no correction is applied to the inelastic rate but an upper limit of 0.25 mb is taken as an additional source of systematic uncertainty.

Low mass diffraction: The T2 acceptance edge at $|\eta| = 6.5$ corresponds approximately to diffractive masses of 3.6 GeV (at 50% efficiency). The contribution of events with all final state particles at $|\eta| > 6.5$ is estimated with QGSJET-II-03 after tuning the Monte Carlo prediction with
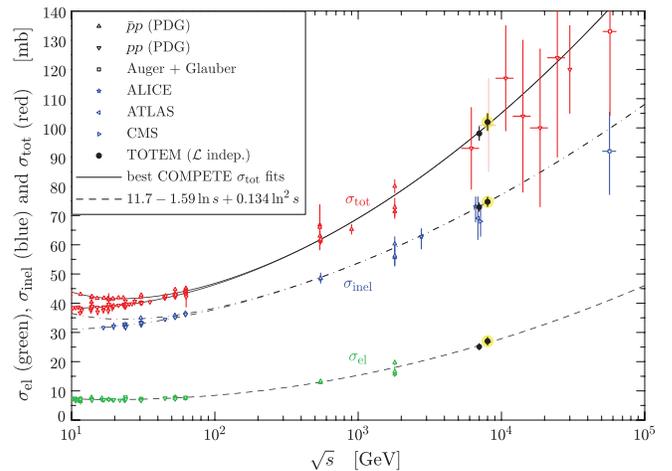

FIG. 1 (color). Compilation [8,20–24] of the total (σ_{tot}), inelastic (σ_{inel}) and elastic (σ_{el}) cross-section measurements: the TOTEM measurements described in this Letter are highlighted. The continuous black lines (lower for pp, upper for $\bar{p}p$) represent the best fits of the total cross-section data by the COMPETE collaboration [19]. The dashed line results from a fit of the elastic scattering data. The dash-dotted lines refer to the inelastic cross section and are obtained as the difference between the continuous and dashed fits.

the observed fraction of 1h events. At 7 TeV this estimation is well in agreement with the indirect measurement of the inelastic cross section [10,12]. To account for the large uncertainty of low mass diffraction and to cover also the other predictions studied [13,15,17], the systematic uncertainty is estimated to be half of the correction, 2.4%.

The total cross section.—The measurements of the total inelastic rate $N_{\rm inel}$ and of the total nuclear elastic rate $N_{\rm el}$ with its extrapolation to $t = 0$, $dN_{\rm el}/dt|_{t=0}$, are combined via the optical theorem to obtain the total cross section [18]

$$\sigma_{\rm tot} = \frac{16\pi}{1 + \rho^2} \frac{(dN_{\rm el}/dt)_{t=0}}{(N_{\rm el} + N_{\rm inel})} \tag{3}$$

yielding the following luminosity-independent measurement:

$$\sigma_{\rm tot} = (101.7 \pm 2.9) \ \text{mb.}$$

The parameter ρ (the ratio of the real to the imaginary part of the forward nuclear elastic amplitude) is assumed to be $= 0.140 \pm 0.007$ from the COMPETE [19] preferred-model extrapolation.

Using the measured (and fully corrected) ratio $N_{\rm el}/N_{\rm inel}$, one can derive the luminosity-and ρ-independent ratios

$$\frac{\sigma_{\rm el}}{\sigma_{\rm inel}} = 0.362 \pm 0.011, \qquad \frac{\sigma_{\rm el}}{\sigma_{\rm tot}} = 0.266 \pm 0.006.$$

The elastic and inelastic cross sections can be derived independently from the luminosity by combining their ratio and sum ($\sigma_{\rm tot}$):

$$\sigma_{\rm el} = (27.1 \pm 1.4) \ \text{mb}, \qquad \sigma_{\rm inel} = (74.7 \pm 1.7) \ \text{mb.}$$

Table IV summarizes the measured cross sections and their detailed uncertainty composition. Figure 1 shows good agreement of the luminosity-independent cross sections measured by the TOTEM collaboration with the extrapolation from lower energies [19].

Summary.—The TOTEM collaboration has measured, for the first time at the LHC, the total proton-proton cross section at $\sqrt{s} = 8$ TeV in a luminosity-independent way. The method was already validated at $\sqrt{s} = 7$ TeV [8]. The two measurements are consistent in terms of detector performance showing comparable systematic uncertainties and they are both in good agreement with the extrapolation of the lower energy measurements.

---

[1] U. Amaldi, R. Biancastelli, C. Bosio, G. Matthiae, J. V. Allaby, W. Bartel, G. Cocconi, A. N. Diddens, R. W. Dobinson, and A. M. Wetherell, Phys. Lett. **44B**, 112 (1973).

[2] U. Amaldi *et al.*, Nucl. Phys. **B145**, 367 (1978).

[3] L. Baksay *et al.*, Nucl. Phys. **B141**, 1 (1978).

[4] R. Battiston *et al.*, Phys. Lett. **117B**, 126 (1982).

[5] N. A. Amos *et al.*, Phys. Lett. B **243**, 158 (1990).

[6] F. Abe *et al.*, Phys. Rev. D **50**, 5550 (1994).

[7] G. Antchev *et al.* (TOTEM Collaboration), Europhys. Lett. **96**, 21002 (2011).

[8] G. Antchev *et al.* (TOTEM Collaboration), Europhys. Lett. **101**, 21004 (2013).

[9] G. Anelli *et al.* (TOTEM Collaboration), JINST **3**, S08007 (2008).

[10] G. Antchev *et al.* (TOTEM Collaboration), Europhys. Lett. **101**, 21002 (2013).

[11] H. Burkhardt, H. Niewiadomski, and F. J. Nemes, Conf. Proc. **C1205201**, 136 (2012).

[12] G. Antchev *et al.* (TOTEM Collaboration), Europhys. Lett. **101**, 21003 (2013).

[13] T. Sjostrand, S. Mrenna, and P. Skands, Comput. Phys. Commun. **178**, 852 (2008).

[14] S. Ostapchenko, Nucl. Phys. B, Proc. Suppl. **151**, 143 (2006).

[15] R. Engel, M. A. Braun, C. Pajares, and J. Ranft, Z. Phys C **74**, 687 (1997).

[16] R. Ciesielski and K. Goulianos, arXiv:1205.1446.

[17] V. A. Khoze, A. D. Martin, and M. G. Ryskin, Phys. Lett. B **679**, 56 (2009).

[18] V. Barone and E. Predazzi, *High-Energy Particle Diffraction* (Springer, Berlin, 2002).

[19] J. R. Cudell, V. Ezhela, P. Gauron, K. Kang, Yu. Kuyanov, S. Lugovsky, E. Martynov, B. Nicolescu, E. Razuvaev, and N. Tkachenko (COMPETE Collaboration), Phys. Rev. Lett. **89**, 201801 (2002).

[20] K. Nakamura *et al.* (Particle Data Group), J. Phys. G **37**, 075021 (2010).

[21] ALICE Collaboration, Report No. CERN-PH-EP-2012-238.

[22] ATLAS Collaboration, Nat. Commun. **2**, 463 (2011).

[23] CMS Collaboration, Report No. CMS-PAS-FWD-11-001; CMS Collaboration, Phys. Lett. B **722**, 5 (2013).

[24] P. Abreu *et al.* (Pierre Auger Collaboration), Phys. Rev. Lett. **109**, 062002 (2012).

G. Antchev,[1] P. Aspell,[2] I. Atanassov,[2,1] V. Avati,[2,*] J. Baechler,[2] V. Berardi,[3,4] M. Berretti,[5,6] E. Bossini,[5,6] U. Bottigli,[6] M. Bozzo,[7,8] E. Brücken,[9,10] A. Buzzo,[7] F. S. Cafagna,[3] M. Calicchio,[3,4] M. G. Catanesi,[3] C. Covault,[11]

M. Csanád,[12,†] T. Csörgő,[12] M. Deile,[2] M. Doubek,[13] K. Eggert,[11] V. Eremin,[14] R. Ferretti,[7,8] F. Ferro,[7]
A. Fiergolski,[15,3] F. Garcia,[9] S. Giani,[2] V. Greco,[6] L. Grzanka,[2,‡] J. Heino,[9] T. Hilden,[9,10] R. A. Intonti,[3] J. Kašpar,[16,2]
J. Kopal,[16,2] V. Kundrát,[16] K. Kurvinen,[9] S. Lami,[5] G. Latino,[6] R. Lauhakangas,[9] T. Leszko,[15] E. Lippmaa,[17]
M. Lokajíček,[16] M. Lo Vetere,[7,8] F. Lucas Rodríguez,[2] M. Macrí,[7] T. Mäki,[9] A. Mercadante,[3,4] N. Minafra,[2]
S. Minutoli,[2,7] F. Nemes,[12,†] H. Niewiadomski,[2] E. Oliveri,[6] F. Oljemark,[9,10] R. Orava,[9,10] M. Oriunno,[2,§]
K. Österberg,[9,10] P. Palazzi,[6] J. Procházka,[16] M. Quinto,[3] E. Radermacher,[6] E. Radicioni,[3] F. Ravotti,[2] E. Robutti,[7]
L. Ropelewski,[2] G. Ruggiero,[2] H. Saarikko,[9,10] A. Santroni,[7,8] A. Scribano,[6] J. Smajek,[2] W. Snoeys,[2] J. Sziklai,[12]
C. Taylor,[11] N. Turini,[6] V. Vacek,[13] M. Vítek,[13] J. Welti,[9,10] J. Whitmore,[18] and P. Wyszkowski[2,‖]

(TOTEM Collaboration)

[1]*INRNE-BAS, Institute for Nuclear Research and Nuclear Energy, Bulgarian Academy of Sciences, Sofia, Bulgaria*
[2]*CERN, Geneva, Switzerland*
[3]*INFN Sezione di Bari, Bari, Italy*
[4]*Dipartimento Interateneo di Fisica di Bari, Bari, Italy*
[5]*INFN Sezione di Pisa, Pisa, Italy*
[6]*Università degli Studi di Siena and Gruppo Collegato INFN di Siena, Siena, Italy*
[7]*INFN Sezione di Genova, Genova, Italy*
[8]*Università degli Studi di Genova, Genova, Italy*
[9]*Helsinki Institute of Physics, Helsinki, Finland*
[10]*Department of Physics, University of Helsinki, Helsinki, Finland*
[11]*Department of Physics, Case Western Reserve University, Cleveland, Ohio, USA*
[12]*MTA Wigner Research Center, RMKI, Budapest, Hungary*
[13]*Czech Technical University, Praha, Czech Republic*
[14]*Ioffe Physical-Technical Institute of Russian Academy of Sciences, St. Petersburg, Russian Federation*
[15]*Warsaw University of Technology, Warsaw, Poland*
[16]*Institute of Physics of the Academy of Sciences of the Czech Republic, Praha, Czech Republic*
[17]*National Institute of Chemical Physics and Biophysics NICPB, Tallinn, Estonia*
[18]*Department of Physics, Penn State University, University Park, Pennsylvania, USA*

*Corresponding author.
  valentina.avati@cern.ch
†Also at Department of Atomic Physics, Eötvös University, Hungary.
‡Visitor from Institute of Nuclear Physics, Polish Academy of Science, Kracow, Poland.
§Present address: SLAC National Accelerator Laboratory, Stanford CA, USA.
‖Visitor from AGH University of Science and Technology, Kracow, Poland.